Effective theory for ultracold strongly interacting fermionic atoms in two dimensions

Fan Wu,[1,*] Jianshen Hu,[1,*] Lianyi He,[1] Xia-Ji Liu,[2] and Hui Hu[2]

[1]*Department of Physics and State Key Laboratory of Low-Dimensional Quantum Physics, Tsinghua University, Beijing 100084, China*

[2]*Centre for Quantum and Optical Science, Swinburne University of Technology, Melbourne, Victoria 3122, Australia*

(Received 20 June 2019; accepted 18 March 2020; published 10 April 2020)

We propose a minimal theoretical model for the description of a two-dimensional (2D) strongly interacting Fermi gas confined transversely in a tight harmonic potential, and present accurate predictions for its zero-temperature equation of state and breathing mode frequency based on existing auxiliary-field quantum Monte Carlo data. We show that the minimal model Hamiltonian needs at least two independent interaction parameters, the 2D scattering length and effective range of interactions, to quantitatively explain recent experimental measurements with ultracold 2D fermions. We resolve in a satisfactory way the puzzling experimental observations of the smaller than expected equations of state and breathing mode frequency. Our establishment of the minimal model for 2D fermions is crucial to understand the Berezinskii-Kosterlitz-Thouless transition in the strongly correlated regime.

DOI: 10.1103/PhysRevA.101.043607

I. INTRODUCTION

Two-dimensional (2D) quantum many-body systems are of great interest due to the interplay of reduced dimensionality and strong correlation, which leads to enhanced quantum and thermal fluctuations [1] and a number of ensuing quantum phenomena such as Berezinskii Kosterlitz Thouless (BKT) physics [2,3]. In this respect, the recently realized 2D Fermi gas of ultracold ^{6}Li and ^{40}K atoms under a tight axial confinement provides a unique platform [4,5], with unprecedented controllability particularly on interatomic interactions. To date, many interesting properties of ultracold 2D Fermi gases have been thoroughly experimentally explored [5], including the equation of state (EoS) at both zero temperature [6,7] and finite temperature [8,9], radio-frequency spectroscopy [10–12], pair momentum distribution [13], first-order correlation function and BKT transition [14], and quantum anomaly in the breathing mode frequency [15–17]. These results may shed light on understanding other important strongly correlated 2D systems, such as high-T_c layered cuprate materials [18], ^{3}He submonolayers [19], exciton-polariton condensates [20], and neutron stars [21].

The present theoretical model of ultracold 2D Fermi gases is simple [4,5]. Under a tight harmonic confinement with trapping frequency ω_z along the axial z axis and a weak confinement $\omega_\perp$ in the transverse direction, the kinematic 2D regime is reached when the number of atoms N is smaller than a threshold $N_{2D} \simeq (\omega_z/\omega_\perp)^2$, so all the atoms are forced into the ground state of the motion along z [5]. The interatomic interactions are then described by a *single* s-wave scattering length a_{2D} [6], which is related to a three-dimensional (3D) scattering length a_{3D} via the quasi-2D scattering amplitude [22]. Various experimental data have been compared and benchmarked with different theoretical predictions of the simple 2D model [23–32]. For EoS, i.e., the chemical potential and pressure at essentially zero temperature, good agreements were found [6,9]. But, at the *quantitative* level the experimental data somehow lie systemically below the accurate predictions from auxiliary-field quantum Monte Carlo (AFQMC) simulations [6,9]. The discrepancy is not so serious and might be viewed as an indicator of small deviation from the 2D kinematics [5], in spite of the fact that the 2D condition $N \ll N_{2D}$ is well satisfied. However, a serious problem does arise when two experimental groups measured the breathing mode frequency in the deep 2D regime most recently [16,17]. The observed frequency turned out to be much smaller than the well-established theoretical prediction in the strongly interacting regime [25,26]. This discrepancy is at the *qualitative* level, suggesting that the simple 2D model with a single parameter a_{2D} may not be sufficient for the description of ultracold 2D Fermi gases [33].

The purpose of this work is to provide a minimal theory of ultracold 2D Fermi gases, with the inclusion of a *properly* defined effective range of interactions. The significant role played by effective range was realized in our previous work [33]. However, there the effective range is taken to be a constant $R_s^{(0)} = -(2\ln 2)a_z^2$, which is *not* reasonable when the interparticle interaction becomes strong (see Fig. 1). Here $a_z \equiv \sqrt{\hbar/(M\omega_z)}$ is the harmonic oscillator length along the z axis. We solve the proposed model Hamiltonian at zero temperature by taking into account strong pair fluctuations at the Gaussian level and beyond (Fig. 2), with the help of a correlation energy from AFQMC in the zero-range limit [30]. This enables us to predict accurate EoS (Figs. 3 and 4), as well as reliable breathing mode frequency (Fig. 5), going beyond the Gaussian approximation considered in our previous work [33]. The puzzling quantitative and qualitative discrepancies, observed in the previous comparisons between experiment and theory [5,6,9,16,17], are therefore naturally resolved in a satisfactory way.

[*]These authors contributed equally to this work.

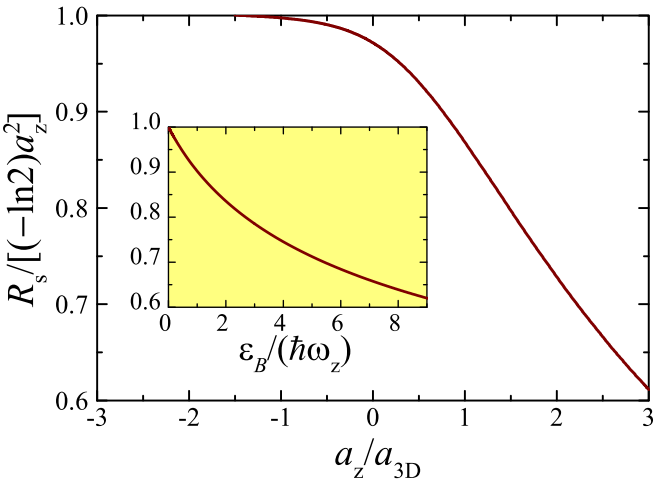

FIG. 1. Confinement-induced effective range of interactions R_s, in units of $R_s^{(0)} = (-\ln 2)a_z^2$, as a function of the inverse 3D scattering length a_z/a_{3D}. The inset shows the effective range as a function of the two-body binding energy.

II. EFFECTIVE RANGE OF INTERACTIONS

We start by considering the collision of two fermions with mass M and unlike spin in a highly anisotropic harmonic trapping potential, described by a quasi-2D scattering amplitude [22],

$$f_{\mathrm{Q2D}}(k; a_{3D}, a_z) = \frac{4\pi}{\sqrt{2\pi}a_z/a_{3D} + \varpi\left(k^2 a_z^2/2\right)}, \tag{1}$$

where the function $\varpi(x)$ has the expansion $\varpi(x \to 0) \simeq -\ln(2\pi x/\mathcal{B}) + (2\ln 2)x + i\pi$ with $\mathcal{B} \simeq 0.905$ [22]. In the simplest treatment, one may parametrize the quasi-2D collision using a 2D scattering length a_{2D} [5,6], by setting the 2D scattering amplitude $f_{2D}(k; a_{2D}) = -2\pi/\ln[ka_{2D}(k)/i] = f_{\mathrm{Q2D}}(k; a_{3D}, a_z)$. In general, one thus obtains a momentum-dependent $a_{2D}(k)$, which in the zero-energy limit takes the form $a_{2D}(k \to 0) = a_s \equiv a_z\sqrt{\pi/\mathcal{B}}\exp(-\sqrt{\pi/2}a_z/a_{3D})$ [22,34]. The advantage of this simple treatment is that the description *universally* depends on a single parameter a_{2D}, to be evaluated at a characteristic collision momentum k_0, i.e., $k_0 = \sqrt{2M\tilde{\mu}}/\hbar$, where $\tilde{\mu}$ is the chemical potential that does not include the two-body binding energy [5,6].

A more adequate parametrization of the 2D collision is to include an effective range of interactions R_s in the 2D scattering amplitude [35]

$$f_{2D}(k; a_s, R_s) = \frac{4\pi}{-2\ln(ka_s) - R_s k^2 + i\pi}, \tag{2}$$

whose pole gives a two-body bound state with binding energy $\varepsilon_B = \hbar^2\kappa^2/M$, where the wave vector κ satisfies $R_s = 2\ln(\kappa a_s)/\kappa^2$. The same two-body bound state should be supported by the pole of the quasi-2D scattering amplitude in Eq. (1) as well. By setting $k \to i\kappa$ there, we find $\sqrt{2\pi}a_z/a_{3D} + \varpi[-\varepsilon_B/(2\hbar\omega_z)] = 0$ [36]. Therefore, we can directly calculate the effective range R_s, once ε_B or κ is solved at a given a_z/a_{3D}.

The effective range obtained in this way is reported in Fig. 1. It decreases monotonically from $R_s^{(0)} \equiv (-\ln 2)a_z^2$ with increasing a_z/a_{3D} (main figure) or binding energy ε_B (inset). We note that $R_s^{(0)}$ can be easily derived from the second expansion term in $\varpi(x \to 0)$ and its magnitude, i.e., $R_s^{(0)} \sim a_z^2$, is a clear indication of the quasi-2D nature of atom collisions [5,22]. As the wave function of two colliding atoms at distance within a_z is set by the full 3D contact interaction potential, these collisions can never be *purely* 2D. They can only be approximately treated as 2D, out of the range $\sim a_z$.

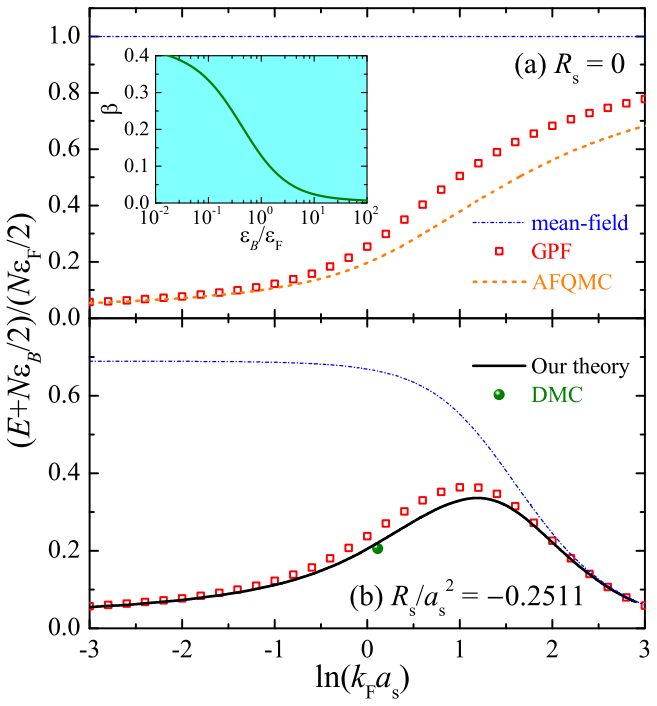

FIG. 2. Total energy with the two-body bound-state energy subtracted as a function of $\ln(k_F a_s)$, at (a) $R_s = 0$ and (b) $R_s \simeq -0.2511a_s^2$. The mean-field and GPF predictions are shown by blue dot-dashed lines and red squares, respectively. At zero range in (a), the latest AFQMC result [30] is plotted by orange dashed line. The inset shows the beta function $\beta = \Delta E_c/\Delta E_{\mathrm{GPF}}$ [see Eq. (4)]. At finite range in (b), our theory (black solid line) is compared to the DMC data (green dot) [38].

III. MANY-BODY THEORY

To account for the effective range R_s, it is useful to adopt a two-channel model [33,37,38]

$$\mathcal{H} = \sum_{\mathbf{k}\sigma=\{\uparrow,\downarrow\}} \xi_{\mathbf{k}} c^\dagger_{\mathbf{k}\sigma} c_{\mathbf{k}\sigma} + \sum_{\mathbf{q}} (2\xi_{\mathbf{q}/2} + \nu) b^\dagger_{\mathbf{q}} b_{\mathbf{q}} + \frac{g}{\sqrt{\mathcal{S}}} \sum_{kq} (b_{\mathbf{q}} c^\dagger_{\mathbf{q}/2+\mathbf{k}\uparrow} c^\dagger_{\mathbf{q}/2-\mathbf{k}\downarrow} + \mathrm{H.c.}), \tag{3}$$

where $\xi_{\mathbf{p}} \equiv \hbar^2\mathbf{p}^2/(2M) - \mu$, and $c_{\mathbf{k}\sigma}$ and $b_{\mathbf{q}}$ are the annihilation operators of atoms and molecules in the open- and closed-channels, respectively. The channel coupling g is related to R_s, via $R_s = -4\pi^2\hbar^4/(M^2 g^2)$, the detuning ν of molecules is tuned to reproduce the binding energy ε_B, i.e., $\nu = -\varepsilon_B + (g^2/\mathcal{S})\sum_{\mathbf{k}}[\hbar^2\mathbf{k}^2/M + \varepsilon_B]^{-1}$ [33,38], and $\mathcal{S}$ is the area.

The two-channel model Hamiltonian has three independently tunable parameters: a_s and R_s related to the interparticle interaction, and also the particle density n [or equivalently Fermi wave vector $k_F = (2\pi n)^{1/2}$]. Therefore, any physical observables of interest can be expressed as functions of two independent *dimensionless* combinations of the three parameters, such as $k_F a_s$ and $k_F^2 R_s$ (or R_s/a_s^2). In the following, to make contact with experiments we will often plot the observables as a function of $\ln(k_F a_s)$, at a given filling factor N/N_{2D}. We note that, the information of the dimensionless effective range, i.e., $k_F^2 R_s$ or R_s/a_s^2, is implicitly contained in the filling factor N/N_{2D}.

It is worth noting, our two-channel Hamiltonian only provides a *mininal* theory of ultracold 2D Fermi gases. For a detailed discussion of its applicability, we refer to Appendix A.

A. Gaussian pair fluctuation approximation and beyond

We solve the model Hamiltonian at different orders of approximation at zero temperature. Formally, the ground-state energy E may be decoupled as

$$E\big[\ln(k_F a_s), k_F^2 R_s\big] = E_{\rm MF} + \Delta E_{\rm GPF} + \Delta E_{\rm c}, \tag{4}$$

where $\varepsilon_F = \hbar^2 k_F^2/(2M)$ is Fermi energy for a system with number density n. The mean-field (MF) theory provides the leading term $E_{\rm MF}$, while the major correction arising from strong pair fluctuations at a Gaussian level can be obtained by using the Gaussian pair fluctuation (GPF) theory [29,33,39–41], i.e., $\Delta E_{\rm GPF} = E_{\rm GPF} - E_{\rm MF}$. The effect of pair fluctuations *beyond* Gaussian level may be characterized by a correlation energy $\Delta E_{\rm c}$, which is anticipated to be much smaller than $\Delta E_{\rm GPF}$. We may fix a correlation energy $\Delta E_{\rm c}$ by requiring the sum of the three contributions in Eq. (4) to coincide with the AFQMC result at zero range $R_s = 0$ [30]. The effective range correction could then be calculated within the GPF theory and approximately taken into account in $\Delta E_{\rm c}$ by assuming that the change in the latter is proportional to the change in the GPF part.

To clarify this idea, in Fig. 2(a) we plot the ground-state energy in the zero-range limit ($R_s = 0$), predicted by mean-field theory, GPF theory [29], and AFQMC simulation [30]. Indeed, the correlation energy given by the difference between the GPF and AFQMC energies is notably smaller than $\Delta E_{\rm GPF}$. In particular, $\Delta E_{\rm c}$ becomes vanishingly small in the tight-binding limit of $\ln(k_F a_s) \to -\infty$ [29]. It is then useful to define a beta function $\beta = \Delta E_{\rm c}/\Delta E_{\rm GPF} \ll 1$, which varies as functions of the two dimensionless interaction parameters $\ln(k_F a_s)$ and $k_F^2 R_s$. For small $k_F^2 R_s$, however, it seems plausible to assume that β relies on $\varepsilon_B/\varepsilon_F$ only, whose dependence can be readily extracted in the zero-range limit using the AFQMC data, as shown in the inset of Fig. 2(a). The other possible choice of the β function is considered in Appendix B.

We thus establish a viable procedure to calculate the ground-state energy at nonzero effective range. For a given set $(k_F a_s, k_F^2 R_s)$, we first calculate the binding energy $\varepsilon_B/\varepsilon_F$ and determine the value of β. Both mean-field and GPF theories are then applied to obtain $E_{\rm MF}$ and $\Delta E_{\rm GPF}$, and consequently $\Delta E_{\rm c} = \beta \Delta E_{\rm GPF}$. In Fig. 2(b), we present $E = E_{\rm GPF} + \Delta E_{\rm c}$ in the black line for a fixed ratio $R_s/a_s^2 \simeq -0.2511$, at which we may benchmark our prediction against available high-precision diffusion Monte Carlo (DMC) data (i.e., the single green dot) [38,42]. We find that the correction $\Delta E_{\rm GPF}$ becomes smaller at nonzero effective range. Towards the noninteracting limit ($a_s \to \infty$) and hence large $k_F^2 R_s$, $\Delta E_{\rm GPF}$ vanishes quickly. This is understandable since pair fluctuations become weaker with decreasing channel coupling g and even mean-field theory may provide an accurate prediction at sufficiently large $k_F^2 R_s$ [38]. The correlation energy also significantly reduces at finite effective range and we find $|\Delta E_{\rm c}| < 0.02 N\varepsilon_F$ at all interaction strengths for $R_s/a_s^2 \simeq -0.2511$. The agreement between our theory with DMC is excellent, with a difference less than $0.01 N\varepsilon_F$.

IV. RESULTS AND DISCUSSIONS

Once the ground-state energy E of a uniform 2D Fermi gas is determined, we calculate directly the chemical potential μ and pressure P using standard thermodynamic relations. Experimentally, these *homogeneous* EoS can be extracted from a low-temperature trapped Fermi gas, by using the local density approximation [43], which assigns a local chemical potential $\mu(r) = \mu_{\rm peak} - V(r)$ to each position r in the potential $V(r) = M\omega_\perp^2 r^2/2$. Both the peak chemical potential $\mu_{\rm peak}$ and the*in situ* density distribution $n(r)$ can be experimentally measured [6,8,9], from which one deduces the homogeneous density EoS $n(\mu)$. By further using the force balance condition [6] $\nabla P(r) = -n(r)\nabla V(r)$, the homogeneous pressure EoS $P(n)$ can also be determined.

To compare to the experimental data, for each data at given magnetic field B, oscillator length a_z, and total number of atoms N, we calculate the 3D s-wave scattering length a_{3D} and then obtain R_s/a_s^2 using Fig. 1. At this fixed R_s/a_s^2, we determine the homogeneous chemical potential μ/ε_F as a function of $\ln(k_F a_s)$ using Fig. 2 and then theoretically generate a density profile for a selected $\mu_{\rm peak}$ (that will be tuned to give the correct total number of atoms N). For more details, see Appendix C 1. In this way, actually, we performed a theoretical simulation under the conditions corresponding to one experimental data point. We finally plot the observable of interest, such as the chemical potential, the pressure or the breathing mode frequency, as a function of $\ln(k_F a_s)$ at a given N/N_{2D}. In other words, we follow exactly the same way as in the experiments to present and characterize our numerical results.

A. Equation of state

In Fig. 3, we show the experimental data for the peak chemical potential $\mu_{\rm peak}$, measured at different magnetic fields (i.e., a_{3D}) and hence at different $\ln(k_F a_s)$ [9,44]. Our predictions for the peak chemical potential, calculated under the same experimental condition, are plotted by the black solid line. We find a good agreement between theory and experiment at $\ln(k_F a_s) > 0$. In contrast, due to the large effective range of interactions in the experiment (i.e., $k_F^2 R_s \lesssim -1.2$ at $N \simeq N_{2D}$ [9]), the zero-range predictions from AFQMC appear to strongly overestimate the chemical potential. This overestimation can partly be removed by using an *effective* energy-dependent a_{2D}, a clever idea first adopted by Turlapov and coworkers [6]. The use of a_{2D} partly accounts for the

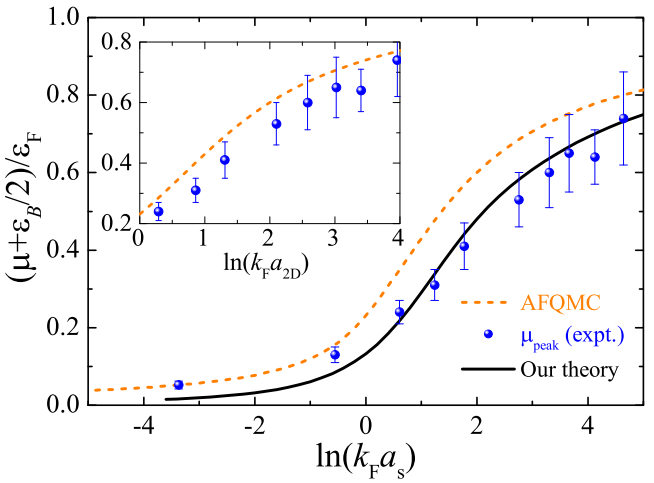

FIG. 3. Chemical potential with the two-body bound-state contribution subtracted, as a function of $\ln(k_F a_s)$ at the number of atoms $N = N_{2D}$. The predictions of AFQMC (i.e., for zero effective range) [30] and our theory with a realistic effective range as in the experiment [9] are shown by orange dashed line and black solid line, respectively, and are compared to the experimental data for μ_{peak} (blue circles) measured at $N \simeq N_{2D}$ [9,44]. The inset shows the chemical potential as a function of $\ln(k_F a_{2D})$, where a_{2D} is the effective scattering length adopted in the experiment [9].

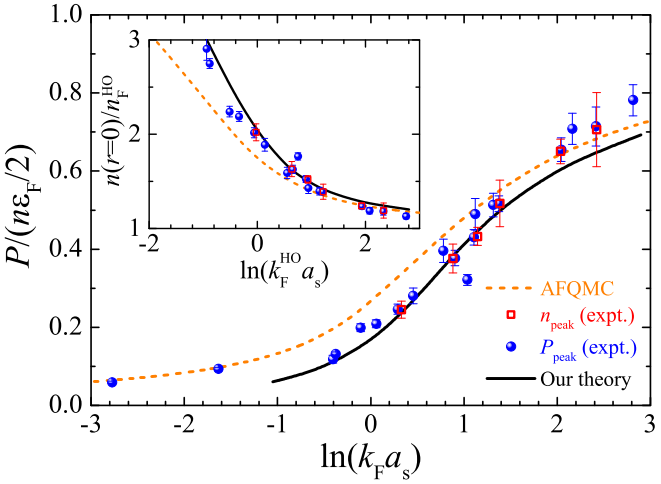

FIG. 4. Pressure as a function of $\ln(k_F a_s)$ at $N = 0.35N_{2D}$. We use blue circles and red squares to show the experimental data from Refs. [6,7] with $N \simeq 0.35N_{2D}$, respectively. The predictions of AFQMC [30] at zero range and our theory at finite range are shown by orange dashed line and black solid line, respectively. Towards the weakly interacting limit, the finite-temperature effect may become sizable and up-shift the pressure data [6]. The inset shows the peak density (in units of n_F^{HO}) as a function of $\ln(k_F^{HO} a_s)$, where n_F^{HO} and $k_F^{HO} = (2\pi n_F^{HO})^{1/2}$ are the peak density and wave vector of an ideal Fermi gas in traps.

confinement-induced effective range in the experiment and leads to a better agreement between AFQMC results and experimental data. As we can see from the inset and also Fig. 1 of Ref. [9], however, there is still a residual discrepancy, which can hardly be understood by possible systematic effects such as finite temperature [45] and the failure of a 2D model due to a finite filling factor N/N_{2D} (see, i.e., Appendixes A 1 and A 2)

In Fig. 4, we present the comparison between our predictions and the experimental data [6,7] for pressure at the trap center. In this case, we have $N \simeq 0.35N_{2D}$ and therefore the effect of the effective range may become weaker. Nevertheless, we can see clearly that in the strongly interacting regime [i.e., $0 < \ln(k_F a_s) < 2$], the experimental data lie systematically below the zero-range results from AFQMC. The model Hamiltonian with a finite effective range should be used to quantitatively understand the experimental measurement. We note that, in harmonic traps the pressure at the center is fixed by the force balance condition to $P = M\omega_\perp^2 N/(2\pi)$ [7]. Using the peak density of an ideal trapped Fermi gas $n_F^{HO} = M\omega_\perp\sqrt{N}/(\pi\hbar)$ [5], we find that the peak density $n \equiv n(r = 0)$ can be written in terms of the pressure at the trap center, i.e., $n/n_F^{HO} = [P/(n\varepsilon_F/2)]^{-1/2}$. This provides an alternative way to illustrate the data, as shown in the inset.

In both Figs. 3 and 4, the agreement between theory and experiment becomes worse at small $k_F a_s$, suggesting the inadequacy of our theory towards the limit of a Bose-Einstein condensate (BEC). This is because, experimentally, the BEC regime is reached by changing a_{3D} instead of k_F. For a small positive a_{3D} the system is better viewed as a quasi-2D weakly interacting BEC, with a 2D scattering length $a_{2D}^{(m)}$ determined from the 3D molecular scattering length $a_{3D}^{(m)} \simeq 0.6a_{3D}$ [46] and with an effective range $R_s^{(m)} \sim -a_z^2$. Our two-channel model cannot fully recover this interaction-driven BEC limit. For more details, we refer to Appendix A.

B. Breathing mode and quantum anomaly

We now turn to consider the breathing mode frequency, which was recently measured in two experiments at $N \sim 0.2N_{2D}$ [16,17], as shown in Fig. 5 by green circles and blue squares. Theoretically, the zero-temperature breathing mode frequency can be conveniently calculated by using the sum-rule approach [47,48]

$$\hbar^2\omega_B^2 = -2\langle r^2\rangle\left[\frac{d\langle r^2\rangle}{d(\omega_\perp^2)}\right]^{-1}, \tag{5}$$

where $\langle r^2\rangle = N^{-1}\int d^2\boldsymbol{r}[r^2 n(r)]$ is the squared radius of the Fermi cloud at a given trapping frequency $\omega_\perp$. In the classical treatment, a 2D Fermi gas is scale-invariant [49] and acquires a polytropic density EoS, $\mu(n) \propto n^2$. As a result, the mode frequency is pinned to $2\omega_\perp$, regardless of temperature and interactions [49]. The deviation of the breathing mode frequency away from $2\omega_\perp$ can be viewed as a quantum anomaly [25,26], arising from strong quantum pair fluctuations in two dimensions [50].

As readily seen from Fig. 5, the observed quantum anomaly in the two experiments is far below the prediction from AFQMC for zero-range interactions with a single 2D scattering length [51]. It can only be understood when we use the proposed minimal model for 2D ultracold fermions and take into account the realistic finite effective range at $N \sim 0.2N_{2D}$. The quantitative difference between our theory and experiment at $0 < \ln(k_F^{HO} a_s) < 1$ could be caused by the finite

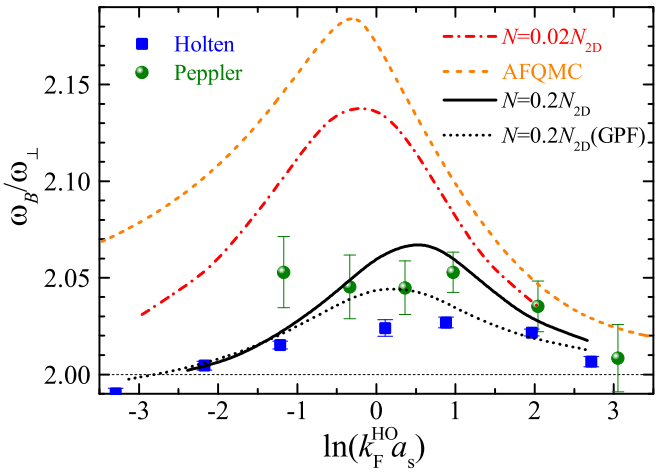

FIG. 5. Breathing mode frequency of 2D strongly interacting fermions as a function of the interaction parameter $\ln(k_F^{HO}a_s)$, at different total number of atoms $N/N_{2D} \to 0$ (AFQMC [51], orange dashed line), 0.02 (red dot-dashed line), and 0.2 (black solid line) as in two recent experiments by Holten *et al.* [16] at 0.10–0.18T_F and $N/N_{2D} \simeq 0.2$ (green circles) and Peppler *et al.* [17] at 0.14–0.22T_F and at $N/N_{2D} \simeq 0.267$ (blue squares). We show also the GPF prediction in the dotted line.

temperature in the two experiments, which is in the range [0.10–0.22]T_F. For a detailed discussion, see Appendix C 3.

It turns out that the breathing mode frequency or quantum anomaly depends sensitively on the effective range. The zero-range result of AFQMC can hardly be asymptotically approached, even if we decrease the number of atoms down to just a few percent of N_{2D} (see the red dot-dashed line at $N = 0.02N_{2D}$). In this case, however, the deviation from the classical limit of $2\omega_\perp$ is very significant and its experimental confirmation is a clear manifestation of quantum anomaly in cold atoms [50,52]. This can be seen more clearly from a colorful contour plot of the breathing mode frequency, as functions of $\ln(k_F^{HO}a_s)$ and N/N_{2D}, as shown in Appendix C 2.

V. CONCLUSION

We established a minimal model to describe ultracold interacting fermions confined in two dimensions and solved it accurately at zero temperature with the help of existing AFQMC results. We showed that the confinement-induced effective range of interactions has to be included to understand the recent measurements on quantum anomaly in a qualitative manner and on equation of state at the quantitative level. Our results pave the way to investigate the crucial role played by effective range in other two-dimensional quantum many-body systems.

ACKNOWLEDGMENTS

We thank I. Boettcher for useful discussions. This research was supported by the National Natural Science Foundation of China, Grant No. 11775123 (L.H.); National Key Research and Development Program of China, Grant No. 2018YFA0306503 (L.H.); and Australian Research Council's (ARC) Discovery Program, Grants No. FT140100003 (X.-J.L), No. DP180102018 (X.-J.L), and No. DP170104008 (H.H.).

APPENDIX A: APPLICABILITY OF OUR EFFECTIVE THEORY

To develop an effective theory for a quasi-2D interacting Fermi gas, it is useful to emphasize that, in cold-atom experiments, the BEC-BCS crossover is driven by tuning the strength of the interatomic interaction, i.e., the 3D scattering length a_{3D}. In the absence of the tight harmonic trapping potential along the z direction, the system is a Fermi superfluid on the BCS side with $a_{3D} < 0$ or in the crossover regime with $a_{3D} \to \pm\infty$, and is a weakly interacting BEC with a molecular scattering length $a_{3D}^{(m)} \simeq 0.6a_{3D}$ in the limit $a_{3D} \to 0^+$ [46]. Upon imposing the tight confinement, the former becomes a 2D Fermi superfluid with an effective range $R_s \sim -O(a_z^2)$, while the latter also correspondingly turns into a weakly interacting 2D BEC with range $R_s^{(m)} \sim -O(a_z^2)$. This is shown in the sketched phase diagram Fig. 6, where the two regimes are divided by a solid boundary line.

As we discuss in detail in the main text, the 2D Fermi superfluid with effective range can be described by a two-channel 2D model Hamiltonian, see Eq. (3) in the main text. However, this model Hamiltonian cannot be used to *accurately* describe the weakly interacting regime of a 2D BEC. This is apparent if we consider the BEC limit of the two-channel 2D model Hamiltonian. We would then obtain a weakly interacting 2D BEC with *zero* range of interactions, instead of a 2D BEC with a finite range $R_s^{(m)} \sim -O(a_z^2)$. The finite range R_s in our fermionic two-channel 2D model will make the 2D molecular scattering length $a_{2D}^{(m)}$ smaller, but it will not induce a finite range at the order of a_z^2. In other words, we need to introduce at least *two* different microscopic model Hamiltonians to describe the strongly interacting 2D Fermi superfluid with effective range [see the area below the solid boundary line in Eq. (6)] and the weakly interacting 2D BEC

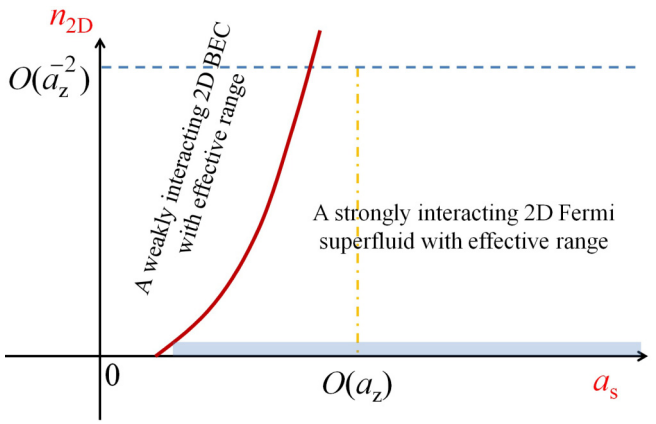

FIG. 6. A sketched phase diagram of a quasi-2D interacting Fermi gas, as functions of 2D scattering length a_s and density n_{2D}. The vertical dot-dashed line shows a_s, at which the 3D scattering length diverges $a_{3D} \to \infty$. The horizontal line is the 2D threshold density, above which the system can no longer be described by a 2D model. In the dilute limit, as shown by the gray area in the plot, a 2D model with a single 2D scattering length a_s might be sufficient.

with effective range (the area above the solid boundary line), respectively.

We note that this is also true in the dilute limit ($n_{2D} \to 0$ or $k_F \to 0$), where one may wish to apply the single-channel model with a single 2D scattering length a_s. In the BEC limit, it is known that the binding energy differs largely from the anticipated value of $\hbar^2/(Ma_s^2)$. The molecular scattering length from the single-channel model is $a_{2D}^{(m)} \simeq 0.56 a_s$ [29] and is different from the result

$$a_{2D}^{(m)} = a_z^{(m)} \sqrt{\frac{\pi}{\mathcal{B}}} \exp\left[-\sqrt{\frac{\pi}{2}} \frac{a_z^{(m)}}{a_{3D}^{(m)}}\right], \tag{A1}$$

following the picture of a weakly interacting quasi-2D BEC in a tight harmonic trapping potential with a 3D scattering length $a_{3D}^{(m)}$ [22]. Here we defined $a_z^{(m)} \equiv \sqrt{\hbar^2/(2M\omega_z)}$ and $a_{3D}^{(m)} \simeq 0.6 a_{3D}$.

At the 2D density $n_{2D} \sim O(a_z^{-2})$ or the Fermi wave vector $k_F \sim O(a_z^{-1})$, we may use the criterion $k_F a_{3D} \sim 1$ or $a_z/a_{3D} \sim 1$ to locate the boundary between the two regimes. Therefore, we find that,

$$[\ln k_F a_s]_c \sim \ln\left[\sqrt{\frac{\pi}{\mathcal{B}}} e^{-\sqrt{\pi/2}}\right] \simeq -0.6. \tag{A2}$$

This threshold value qualitatively explains why in Figs. 3 and 4 of the main text, the agreement between the theory and experiment becomes worse at small $k_F a_s$.

1. Dependence on N/N_{2D}

Strictly speaking, any 2D model is valid in the dilute limit only, with $N \ll N_{2D}$. However, we may use the 2D model up to $N \sim N_{2D}$ if the correction due to the quasi-2D configuration is small. Here we check this idea within the mean-field framework, using the full mean-field solutions at the 3D-2D-dimensional crossover in Ref. [33] as a benchmark.

In Fig. 7, we report the 2D number density n_{2D} as a function of the chemical potential μ, at $a_z/a_{3D} = -0.5$ [Fig. 7(a)] and $a_z/a_{3D} = 0$ [Fig. 7(b)], predicted by mean-field theory for different microscopic models. The black solid lines are the full solution (i.e., the benchmark results) by fully considering the tight harmonic trapping potential along the z axis (with the energy scale $\hbar\omega_z$), while the predictions of our effective two-channel 2D model are shown by green stars. Here we anticipate the minimum chemical potential is given by $\mu_m = \hbar\omega_z/2 - \varepsilon_B/2$, where the two-body binding energy ε_B is set by a_z/a_{3D}, and the condition $N \sim N_{2D}$ roughly corresponds to $\mu \sim 1.5\hbar\omega_z$.

We find that there is a fairly good agreement between the full solution and the approximate solution from the effective two-channel 2D model. In particular, at $a_z/a_{3D} = 0$ and $\mu = 1.5\hbar\omega_z$, the *relative* error due to the use of effective two-channel 2D model is about 10%. This means that at the 2D BEC-BCS crossover regime (which corresponds to $a_z/a_{3D} = 0$), the relative error in the chemical potential shown in Fig. 3 of the main text is about 10%, due to the imperfect 2D condition $N \sim N_{2D}$. This gives an absolute error in the chemical potential $\sim 0.03\varepsilon_F$.

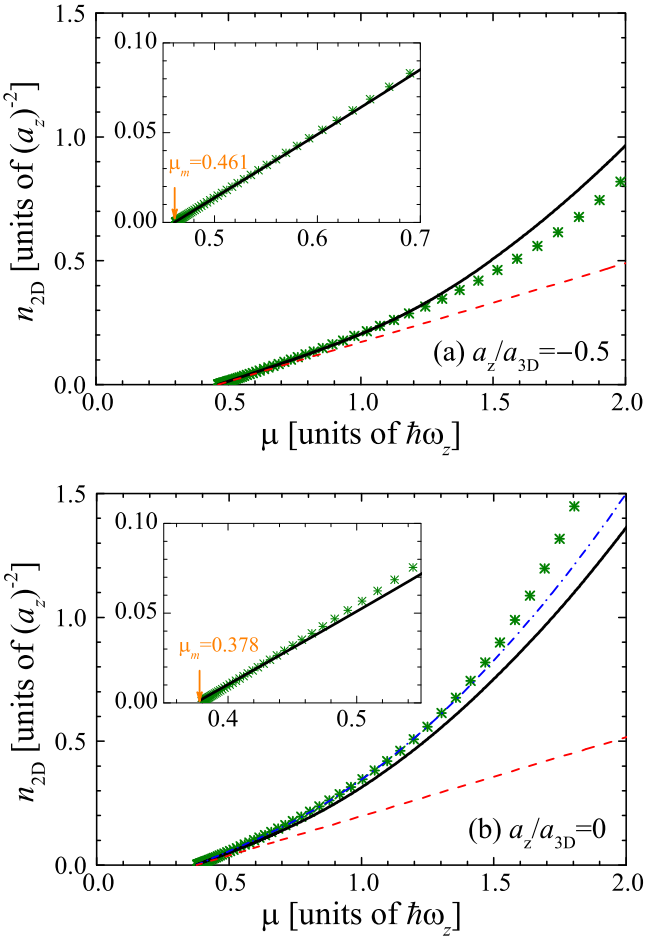

FIG. 7. The 2D number density n_{2D} as a function of the chemical potential μ, at (a) $a_z/a_{3D} = -0.5$ and (b) $a_z/a_{3D} = 0$, predicted by mean-field theories. The insets highlight the areas with small chemical potential or density. Here the black solid lines are from the mean-field calculations, fully taking into account the tight harmonic trapping potential (i.e., $n_{2D}^{(\mathrm{full})}(\mu)$ [33]) and the symbol green stars are the mean-field results obtained by using our effective theory [i.e., $n_{2D}^{(2c)}(\mu)$ from the two-channel 2D model Hamiltonian in Eq. (3) in the main text]. We report also the the mean-field results of the single-channel model, $n_{2D}^{(\mathrm{sc})}(\mu) = M(\mu - \mu_m)/\hbar^2$, in red dashed lines. In (b), the blue dot-dashed line shows the result $1.1 n_{2D}^{(\mathrm{full})}(\mu)$.

2. Finite-temperature correction to equation of state

In the main text, we focus on the zero-temperature case and neglect any temperature dependence of the equations of state. This sounds reasonable, as the typical temperature in the experiments is about 0.05–0.1T_F [6,9] and we anticipate the finite-temperature correction is small. Theoretically, however, a finite-temperature 2D interacting Fermi gas is very difficult to handle and we can hardly have solid results on the finite-temperature effect. One exception is the recent theoretical breakthrough in the constrained-path auxiliary-field quantum Monte Carlo (AFQMC) method [45]. The finite-temperature generalization leads to the accurate determination of the chemical potential at $\ln(k_F a_s) \sim 4$ for temperatures up to $0.125T_F$. The finite-temperature correction to the chemical potential is indeed found to be small, with $\Delta\mu \sim 0.02\varepsilon_F$ at $T = 0.125T_F$ [45]. We anticipate that the finite-temperature

correction at other interaction parameters (i.e., $\ln(k_F a_s) \in [0, 4]$) is similar.

APPENDIX B: CHOICE OF THE β FUNCTION

To obtain the correlation energy ΔE_c beyond the GPF approximation, a beta function $\beta = \Delta E_c / \Delta E_{\rm GPF}$ is introduced in the main text, where $\Delta E_{\rm GPF} \equiv E_{\rm GPF} - E_{\rm MF}$. There are different ways to choose the beta function. However, as a result of the smallness of the beyond-GPF correlation energy, different choices may only lead to negligible corrections to the equation of state. To show this, let us consider two different choices: (1) the beta function depends on the two-body binding energy, i.e., $\varepsilon_B/\varepsilon_F$, which is a function of $\ln(k_F a_s)$ and $k_F^2 R_s$. This choice is used in the main text. (2) On the other hand, we may assume that the beta function depends on $\ln(k_F a_s)$ only. This choice neglects the dependence on the effective range and should be worse than the first choice.

In Fig. 8, we show the energy, as a result of the two different choices of the beta function, at different values R_s/a_s^2 (or at different $a_z/a_{\rm 3D}$). The energy differences between the two choices are highlighted in the insets. They are indeed very small, at the order of $0.001\varepsilon_F$. Therefore, we believe that our results on the chemical potential, pressure equation of state, and breathing mode frequency depend very weakly on the choice of the beta function.

APPENDIX C: QUANTUM ANOMALY IN BREATHING MODE

1. Density profiles

The breathing mode frequency is calculated with the sum-rule approach, using density profiles as the input (for the purpose of calculating the cloud width). Density profile can be determined by using the local density approximation, based on the homogeneous equation of state $n(\mu)$ beyond the GPF approximation for the two-channel 2D model Hamiltonian (see Fig. 2 in the main text). That is, we assume a local chemical potential $\mu(r) = \mu_{\rm peak} - V(r)$ for each position r in the harmonic trapping potential $V(r) = M\omega_\perp^2 r^2/2$. Here $\mu_{\rm peak}$ is the peak chemical potential. At position r, we then obtain the local density $n(r) = n[\mu(r)]$. We finally adjust the peak chemical potential to yield the total number of atoms N, i.e., $N = \int d\mathbf{r} n(r)$.

In Fig. 9, we show the density profiles at a different value of R_s/a_s^2, which corresponds to different values of the interaction strength (i.e., $a_z/a_{\rm 3D}$). We consider the experimental situation with number of atoms $N = 0.20 N_{\rm 2D}$. With decreasing R_s/a_s^2, i.e., crossing from the BCS side to the BEC side, the peak density increases and the cloud radius decreases.

2. $N/N_{\rm 2D}$ dependence of the breathing mode frequency

In Fig. 10, we report the breathing mode frequency as functions of $\ln(k_F^{\rm HO} a_s)$ and of $N/N_{\rm 2D}$, in the form of a contour plot. The number of atoms $N/N_{\rm 2D}$ is shown in the logarithmic scale. We note that, a notable quantum anomaly, i.e., $\omega_B > 2.1\omega_\perp$, only shows up at $N \sim 0.01 N_{\rm 2D}$ for interaction parameter $-1.0 < \ln(k_F^{\rm HO} a_s) < 0.5$.

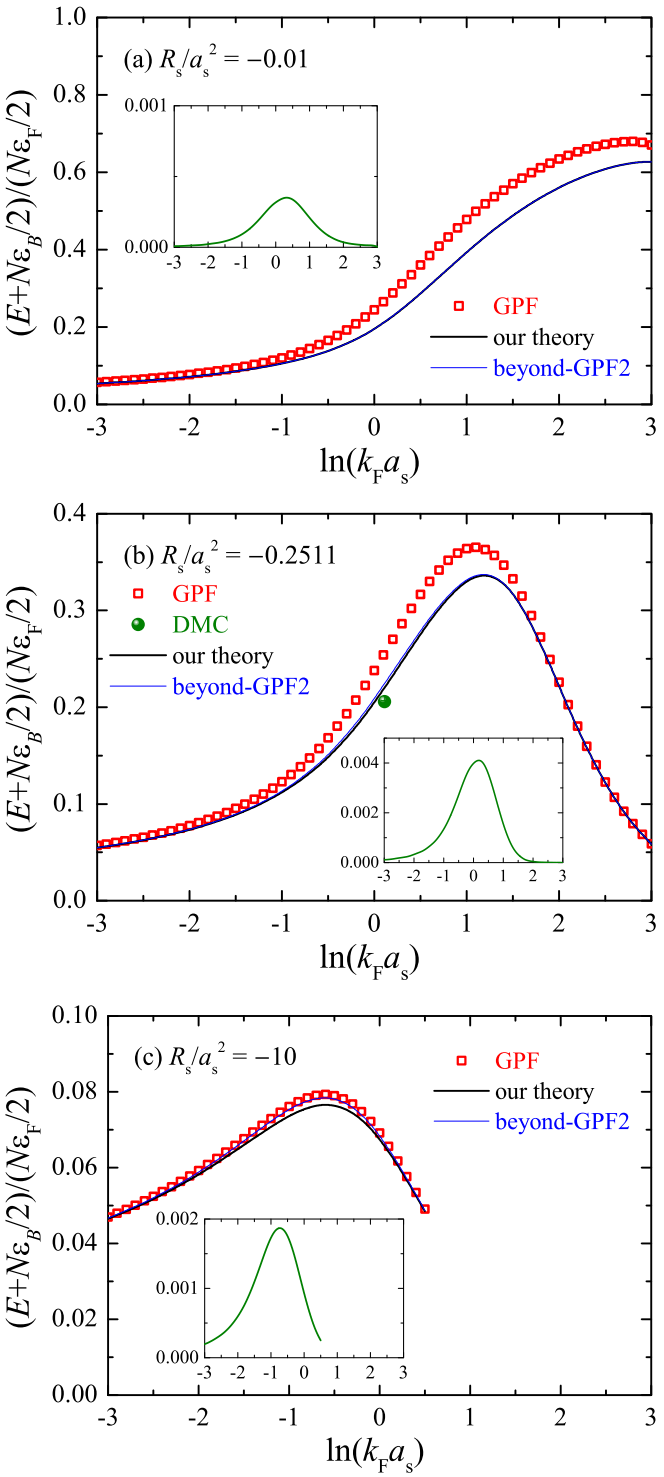

FIG. 8. Energy as a function of $\ln(k_F a_s)$ at different values of $R_s/a_s^2 =$ (a) -0.01, (b) -0.2511, and (c) -10, as a result of the different choices for the beta function $\beta = \Delta E_c/\Delta E_{\rm GPF}$: (1) the beta function depends on $\varepsilon_B/\varepsilon_F$ (thick black lines, labeled as "our theory"); (2) the beta function depends on $\ln(k_F a_s)$ only (blue thin lines, labeled as "beyond-GPF2"); (3) we neglect completely the correlation energy beyond GPF (i.e., red squares, labeled as "GPF"). The insets show the difference between choices (1) and (2).

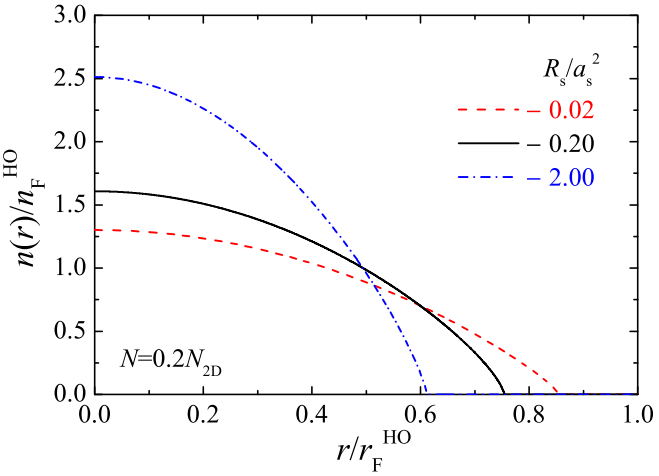

FIG. 9. Zero-temperature density profiles at different values of $R_s/a_s^2 = -0.02$ (red dashed line), -0.20 (black solid line), and -2.00 (blue dot-dashed line) and at $N = 0.20N_{2D}$. The corresponding dimensionless interaction parameters are $\ln(k_F^{HO}a_s) \simeq 1.715$, 0.551, and -0.654, respectively. Here k_F^{HO} is the Fermi wave vector of an ideal Fermi gas in harmonic traps. The density and radius are measured in units of $n_F^{HO} = (1/\pi)\sqrt{N/N_{2D}}a_z^{-2}$ and $r_F^{HO} = \sqrt{2N}(N/N_{2D})^{-1/4}a_z$, respectively.

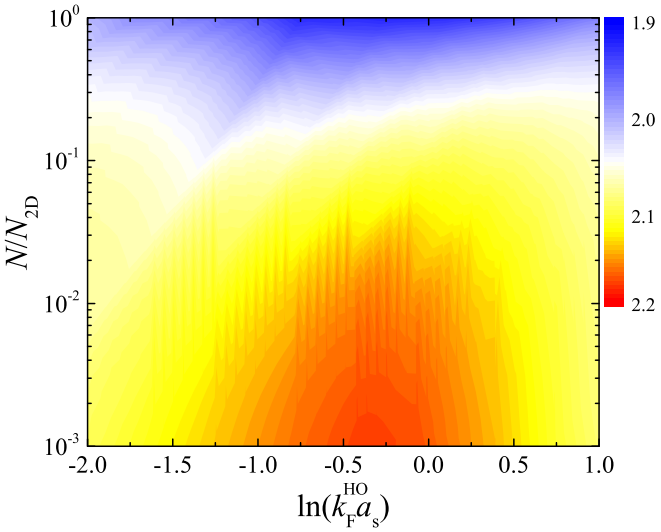

FIG. 10. Contour plot of the breathing mode frequency of 2D strongly interacting fermions, as functions of the interaction parameter $\ln(k_F^{HO}a_s)$ and of the total number of atoms N/N_{2D} (in the logarithmic scale), predicted by our two-channel 2D model beyond GPF.

3. Finite-temperature effect on the breathing mode frequency

Let us now consider the possible finite-temperature effect on the breathing mode frequency. The calculation of the breathing mode of a 2D interacting Fermi gas at a *small* but finite temperature is difficult, due to the *insufficient* knowledge on the equation of state. To have a rough picture on the finite-temperature effect, alternatively we may consider the breathing mode of a one-dimensional (1D) s-wave interacting Bose gas (which is equivalent to a 1D p-wave interacting Fermi gas) [48], where the equation of state can be solved by using thermodynamic Bethe Ansatz.

As shown in Fig. 4(b) of Ref. [48], in the *strongly interacting* regime [i.e., the curve with $N(a_{1D}/a_{ho})^2 = 1$], the breathing mode frequency increases from $1.819\omega_0$ to $1.844\omega_0$, when the temperature of the system increases from 0 to $0.2T_F$. Here ω_0 is the trapping frequency. Therefore, the change in the breathing mode frequency is about 0.025 trapping frequency, when the temperature fluctuates about $0.2T_F$. We may anticipate the similar temperature effect for a 2D interacting Fermi gas in the strongly interacting regime. Thus we estimate that, for the experiments at Heidelberg [16] and Swinburne Universities [17], a finite temperature in the range $[0.10–0.22]T_F$ may lead to a change in the breathing mode frequency at about $\Delta\omega_B \sim 0.02\omega_\perp$.

[1] M. Randeria, J.-M. Duan, and L.-Y. Shieh, Bound States, Cooper Pairing, and Bose Condensation in Two Dimensions, Phys. Rev. Lett. **62**, 981 (1989).

[2] V. L. Berezinskii, Destruction of long-range order in one-dimensional and two-dimensional systems with a continuous symmetry group. II. Quantum systems, Sov. Phys. JETP **34**, 610 (1972) [Zh. Eksp. Teor. Fiz. **61**, 1144 (1971)].

[3] J. M. Kosterlitz and D. J. Thouless, Ordering, metastability and phase transitions in two-dimensional systems, J. Phys. C **6**, 1181 (1973).

[4] J. Levinsen and M. M. Parish, Strongly interacting twodimensional Fermi gases, in *Annual Review of Cold Atoms and Molecules*, Vol. 3 (World Scientific, Singapore, 2015), Chap. 1, pp. 1–75.

[5] A. V. Turlapov and M. Y. Kagan, Fermi-to-Bose crossover in a trapped quasi-2D gas of fermionic atoms, J. Phys.: Condens. Matter **29**, 383004 (2017).

[6] V. Makhalov, K. Martiyanov, and A. Turlapov, Ground-State Pressure of Quasi-2D Fermi and Bose Gases, Phys. Rev. Lett. **112**, 045301 (2014).

[7] K. Martiyanov, T. Barmashova, V. Makhalov, and A. Turlapov, Pressure profiles of nonuniform two-dimensional atomic Fermi gases, Phys. Rev. A **93**, 063622 (2016).

[8] K. Fenech, P. Dyke, T. Peppler, M. G. Lingham, S. Hoinka, H. Hu, and C. J. Vale, Thermodynamics of an Attractive 2D Fermi Gas, Phys. Rev. Lett. **116**, 045302 (2016).

[9] I. Boettcher, L. Bayha, D. Kedar, P. A. Murthy, M. Neidig, M. G. Ries, A. N. Wenz, G. Zürn, S. Jochim, and T. Enss, Equation of State of Ultracold Fermions in the 2D BEC-BCS Crossover Region, Phys. Rev. Lett. **116**, 045303 (2016).

[10] B. Fröhlich, M. Feld, E. Vogt, M. Koschorreck, W. Zwerger, and M. Köhl, Radio-Frequency Spectroscopy of a Strongly Interacting Two-Dimensional Fermi Gas, Phys. Rev. Lett. **106**, 105301 (2011).

[11] A. T. Sommer, L. W. Cheuk, M. J. H. Ku, W. S. Bakr, and M. W. Zwierlein, Evolution of Fermion Pairing from Three to Two Dimensions, Phys. Rev. Lett. **108**, 045302 (2012).

[12] Y. Zhang, W. Ong, I. Arakelyan, and J. E. Thomas, Polaron-to-Polaron Transitions in the Radio-Frequency Spectrum of a Quasi-Two-Dimensional Fermi Gas, Phys. Rev. Lett. **108**, 235302 (2012).

[13] M. G. Ries, A. N. Wenz, G. Zürn, L. Bayha, I. Boettcher, D. Kedar, P. A. Murthy, N. Neidig, T. Lompe, and S. Jochim, Observation of Pair Condensation in the Quasi-2D BEC– BCS Crossover, Phys. Rev. Lett. **114**, 230401 (2015).

[14] P. A. Murthy, I. Boettcher, L. Bayha, M. Holzmann, D. Kedar, M. Neidig, M. G. Ries, A. N. Wenz, G. Zürn, and S. Jochim, Observation of the Berezinskii– Kosterlitz– Thouless Phase Transition in an Ultracold Fermi Gas, Phys. Rev. Lett. **115**, 010401 (2015).

[15] E. Vogt, M. Feld, B. Fröhlich, D. Pertot, M. Koschorreck, and M. Köhl, Scale Invariance and Viscosity of a Two-Dimensional Fermi Gas, Phys. Rev. Lett. **108**, 070404 (2012).

[16] M. Holten, L. Bayha, A. C. Klein, P. A. Murthy, P. M. Preiss, and S. Jochim, Anomalous Breaking of Scale Invariance in a Two-Dimensional Fermi Gas, Phys. Rev. Lett. **121**, 120401 (2018).

[17] T. Peppler, P. Dyke, M. Zamorano, S. Hoinka, and C. J. Vale, Quantum Anomaly and 2D-3D Crossover in Strongly Interacting Fermi Gases, Phys. Rev. Lett. **121**, 120402 (2018).

[18] V. M. Loktev, R. M. Quick, and S. G. Sharapov, Phase fluctuations and pseudogap phenomena, Phys. Rep. **349**, 1 (2001).

[19] M. Ruggeri, S. Moroni, and M. Boninsegni, Quasi-2D Liquid ^{3}He, Phys. Rev. Lett. **111**, 045303 (2013).

[20] H. Deng, H. Haug, and Y. Yamamoto, Exciton-polariton Bose-Einstein condensation, Rev. Mod. Phys. **82**, 1489 (2010).

[21] J. A. Pons, D. Viganó, and N. Rea, A highly resistive layer within the crust of x-ray pulsars limits their spin periods, Nat. Phys. **9**, 431 (2013).

[22] D. S. Petrov and G. V. Shlyapnikov, Interatomic collisions in a tightly confined Bose gas, Phys. Rev. A **64**, 012706 (2001).

[23] G. Bertaina and S. Giorgini, BCS-BEC Crossover in a Two-Dimensional Fermi Gas, Phys. Rev. Lett. **106**, 110403 (2011).

[24] A. A. Orel, P. Dyke, M. Delehaye, C. J. Vale, and H. Hu, Density distribution of a trapped two-dimensional strongly interacting Fermi gas, New J. Phys. **13**, 113032 (2011).

[25] J. Hofmann, Quantum Anomaly, Universal Relations, and Breathing Mode of a Two-Dimensional Fermi Gas, Phys. Rev. Lett. **108**, 185303 (2012).

[26] E. Taylor and M. Randeria, Apparent Low-Energy Scale Invariance in Two-Dimensional Fermi Gases, Phys. Rev. Lett. **109**, 135301 (2012).

[27] M. Bauer, M. M. Parish, and T. Enss, Universal Equation of State and Pseudogap in the Two-Dimensional Fermi Gas, Phys. Rev. Lett. **112**, 135302 (2014).

[28] M. Barth and J. Hofmann, Pairing effects in the nondegenerate limit of the two-dimensional Fermi gas, Phys. Rev. A **89**, 013614 (2014).

[29] L. He, H. Lü, G. Cao, H. Hu, and X.-J. Liu, Quantum fluctuations in the BCS-BEC crossover of two-dimensional Fermi gases, Phys. Rev. A **92**, 023620 (2015).

[30] H. Shi, S. Chiesa, and S. Zhang, Ground-state properties of strongly interacting Fermi gases in two dimensions, Phys. Rev. A **92**, 033603 (2015).

[31] B. C. Mulkerin, K. Fenech, P. Dyke, C. J. Vale, X.-J. Liu, and H. Hu, Comparison of strong-coupling theories for a two-dimensional Fermi gas, Phys. Rev. A **92**, 063636 (2015).

[32] E. R. Anderson and J. E. Drut, Pressure, Compressibility, and Contact of the Two-Dimensional Attractive Fermi Gas, Phys. Rev. Lett. **115**, 115301 (2015).

[33] H. Hu, B. C. Mulkerin, U. Toniolo, L. He, and X.-J. Liu, Reduced Quantum Anomaly in a Quasi-Two-Dimensional Fermi Superfluid: Significance of the Confinement-Induced Effective Range of Interactions, Phys. Rev. Lett. **122**, 070401 (2019).

[34] The definition of a 2D scattering length (denoted by a_2) used by Turlapov group in Refs. [6,7] is slightly different, and is related to $a_{2D}(k_0)$ by, $a_{2D}(k_0) = (e^{\gamma_E}/2)a_2$, where $\gamma_E \simeq 0.577$ is Euler's constant and $k_0 = \sqrt{2M\tilde{\mu}}/\hbar$. We also note that, in Ref. [33] we used the notation $a_{2D} = a_{2D}(k \to 0)$, which is exactly a_s defined in this work.

[35] S. K. Adhikari, Quantum scattering in two dimensions, Am. J. Phys. **54**, 362 (1986).

[36] This equation can be rewritten as $a_z/a_{3D} = \mathcal{F}[\varepsilon_B/(\hbar\omega_z)]$, where the function $\mathcal{F}(x)$ is given by $\mathcal{F}(x) = \int_0^\infty du(4\pi u^3)^{-1/2}[1 - e^{-xu}/\sqrt{(1-e^{-2u})/(2u)}]$.

[37] X.-J. Liu and H. Hu, Self-consistent theory of atomic Fermi gases with a Feshbach resonance at the superfluid transition, Phys. Rev. A **72**, 063613 (2005).

[38] L. M. Schonenberg, P. C. Verpoort, and G. J. Conduit, Effective-range dependence of two-dimensional Fermi gases, Phys. Rev. A **96**, 023619 (2017).

[39] H. Hu, X.-J. Liu, and P. D. Drummond, Equation of state of a superfluid Fermi gas in the BCS-BEC crossover, Europhys. Lett. **74**, 574 (2006).

[40] H. Hu, P. D. Drummond, and X.-J. Liu, Universal thermodynamics of strongly interacting Fermi gases, Nat. Phys. **3**, 469 (2007).

[41] R. B. Diener, R. Sensarma, and M. Randeria, Quantum fluctuations in the superfluid state of the BCS-BEC crossover, Phys. Rev. A **77**, 023626 (2008).

[42] The DMC simulations in Ref. [38] were carried out as a function of $k_F^2 r_{\rm eff}^2 = 4k_F^2 R_s/\pi$ in the strongly interacting regime, where the mean-field solution for chemical potential $\mu_{\rm MF}$ is fixed to 0. By solving the mean-field equation, we find the following relation between the effective range and 2D scattering length: $1/(k_F a_s) = [(\sqrt{1-4k_F^2 R_s} - 1)/(-2k_F^2 R_s)]^{1/2}$. The green dot in Fig. 2(b) corresponds to the DMC data at $k_F^2 r_{\rm eff}^2 = -0.4$, leading to $k_F^2 R_s \simeq -0.31416$ and $k_F a_s \simeq 1.1185$. This gives the ratio $R_s/a_s^2 \simeq -0.2511$.

[43] D. A. Butts and D. S. Rokhsar, Phys. Rev. A **55**, 4346 (1997).

[44] We used the peak chemical potential data $\tilde{\mu}_0 = \mu_{\rm peak} + \varepsilon_B/2$ listed in Table III of the Supplemental Material of Ref. [9]. To have a robust procedure of measurement, in the experiment the chemical potential with the two-body binding energy subtracted ($\tilde{\mu}$) was assumed to be proportional to the local Fermi energy $\tilde{\mu} = \varepsilon_F/c$ [9]. A ratio $1/c$ was then obtained by fitting the linear relation at different densities and was supposed to provide the same information as $\mu_{\rm peak}$ at the trap center. The ratio $1/c$ is slightly smaller than $\tilde{\mu}_0/\varepsilon_F$, and is plotted in Fig. 1 of Ref. [9].

[45] Y.-Y. He, H. Shi, and S. Zhang, Reaching the Continuum Limit in Finite-Temperature *Ab Initio* Field-Theory Computations in Many-Fermion Systems, Phys. Rev. Lett. **123**, 136402 (2019).

[46] D. S. Petrov, C. Salomon, and G. V. Shlyapnikov, Weakly Bound Dimers of Fermionic Atoms, Phys. Rev. Lett. **93**, 090404 (2004).

[47] C. Menotti and S. Stringari, Collective oscillations of a one-dimensional trapped Bose-Einstein gas, Phys. Rev. A **66**, 043610 (2002).

[48] H. Hu, G. Xianlong, and X.-J. Liu, Collective modes of a one-dimensional trapped atomic Bose gas at finite temperatures, Phys. Rev. A **90**, 013622 (2014).

[49] L. P. Pitaevskii and A. Rosch, Breathing modes and hidden symmetry of trapped atoms in two dimensions, Phys. Rev. A **55**, R853(R) (1997).

[50] M. Olshanii, H. Perrin, and V. Lorent, Example of a Quantum Anomaly in the Physics of Ultracold Gases, Phys. Rev. Lett. **105**, 095302 (2010).

[51] We calculated the density profile by using the AFQMC EoS and have then used the sum-rule equation (5) to determine the breathing mode frequency within AFQMC. This calculation improves the previous estimation given in Refs. [25,26].

[52] P. A. Murthy, N. Defenu, L. Bayha, M. Holten, P. M. Preiss, T. Enss, and S. Jochim, Quantum scale anomaly and spatial coherence in a 2D Fermi superfluid, Science **365**, 268 (2019).